

Description of bulk observables in Au+Au collisions at top RHIC energy in the integrated HydroKinetic Model

M. D. Adzhymambetov¹, V. M. Shapoval¹, and Yu. M. Sinyukov¹

¹*Bogolyubov Institute for Theoretical Physics, 03143 Kiev, Ukraine*

Abstract

The results on the main bulk observables obtained in the simulations within the integrated hydrokinetic model (iHKM) of Au+Au collisions at the RHIC energy $\sqrt{s_{NN}} = 200$ GeV are presented along with the corresponding experimental data from the STAR and the PHENIX collaborations. The simulations include all the stages of the collision process: formation of the initial state, its gradual thermalization and hydrodynamization, viscous relativistic hydro-evolution, system's hadronization and particlization, and, finally, an expansion of the interacting hadron-resonance gas. The model gives a satisfactory description of charged-particle multiplicities, particle number ratios, transverse momentum spectra for pions, kaons, protons and antiprotons, charged-particle v_2 coefficients, and femtoscopy radii at all collision centralities. It is demonstrated how one can estimate the times of the pion and kaon maximal emission from the femto-scales.

PACS numbers: 13.85.Hd, 25.75.Gz

Keywords: *gold-gold collisions, RHIC, multiplicity, momentum spectra, interferometry radii*

I. INTRODUCTION

The comprehensive study of ultrarelativistic heavy ion collisions allow researchers gradually, step by step reveal new properties of rather interesting and unusual form of matter, created in these processes, and construct more and more clear and full picture of evolution of such super dense and super hot systems. As it became clear after the thorough analysis of bulk observables at RHIC and LHC, such as particle multiplicities, transverse momentum spectra, and femtoscopy scales, the strongly interacting quark-gluon matter, formed in a collision at high energy, at some stage of its evolution undergoes collective expansion and behaves like a nearly thermalized, (quasi)macroscopic system. This fact justified the application of hydrodynamical and statistical mechanics approximations for the theoretical description of this stage. However, the pre-thermal dynamics, leading to the system's thermalization, as well as the “afterburner” stage of its evolution, also play an important role in the formation of final observables. That is why a realistic model, allowing to successfully describe and predict various experimental data and helping to understand the reasons and mechanisms for the specific experiment results, should be complex and include an adequate simulation of all the stages of the collision process.

In this work, we present the results of our study, devoted to the description of different bulk observables in Au+Au collisions at the RHIC energy $\sqrt{s_{NN}} = 200$ GeV within such a decent model — the integrated hydrokinetic model [1] (iHKM).

Despite the experiments at the top RHIC energy were performed quite a long time ago, and the most recent results concern heavy ion collisions at the LHC, the datasets, collected at RHIC, are still in use and still are of interest for the analysis, in particular, for the studies dealing with kaon femtoscopy [2]. Additionally, although the time has passed since the first papers, presenting the results of certain measurements at RHIC (e.g., two-pion femtoscopy), were published, the STAR and PHENIX collaborations continue to issue new articles, containing results on the same topic, but with increased accuracy, in a wider region, with new cuts applied, etc. This fact also motivates one not to forget about the RHIC data.

Previously, the Au+Au collisions at the top RHIC energy were successfully simulated in the hydrokinetic model [3–5], the model-predecessor of the modern, more developed iHKM,

which proved to be good in describing observables at the LHC energies [1, 6, 7]. Here we aim to adjust the iHKM to the description of yields, p_T spectra, interferometry radii, etc. at RHIC and see what differences in the model parameters and tuning will it require as compared to the LHC case.

II. MODEL DESCRIPTION

In iHKM the process of the evolution of the system, formed in the relativistic nuclear collision starts with the pre-thermal stage, which simulates the process of gradual transformation of the initially not thermalized system to a nearly thermal one, close to local thermal and chemical equilibrium, that can be further described using viscous hydrodynamics approximation. At this stage an energy-momentum transport approach in the relaxation time approximation is utilized (see [1, 8] for details).

The initial distribution of energy density in the transverse plane for the pre-thermal stage is chosen to be a linear combination of wounded nucleons and binary collision contributions in GLISSANDO [9] Glauber Monte Carlo model:

$$\epsilon(b, \mathbf{r}_T) = \epsilon_0(\tau_0) \frac{(1 - \alpha)N_w(b, \mathbf{r}_T)/2 + \alpha N_{bin}(b, \mathbf{r}_T)}{(1 - \alpha)N_w(b = 0, \mathbf{r}_T = 0)/2 + \alpha N_{bin}(b = 0, \mathbf{r}_T = 0)}, \quad (1)$$

where the parameters α (defining the proportion between the two contributions to $\epsilon(b, \mathbf{r}_T)$) and $\epsilon_0(\tau_0)$ (defining the maximal initial energy density in the center of the system for the most central collisions) are adjusted to provide the best fit to experimental dependence of mean charged particle multiplicity in the pseudorapidity region $|\eta| < 0.5$ on centrality, and the value of the starting time τ_0 ensures the best description of pion p_T spectrum slope in the most central events. For the current study we obtained $\alpha = 0.18$ and $\epsilon_0 = 235 \text{ GeV/fm}^3$ at $\tau_0 = 0.1 \text{ fm}/c$. At the LHC energies, the coefficient $\alpha = 0.24$, and at the same initial time $\tau_0 = 0.1 \text{ fm}/c$ one has $\epsilon_0 = 679 \text{ GeV/fm}^3$ for $\sqrt{s_{NN}} = 2.76 \text{ TeV}$ [1], and $\epsilon_0 = 1067 \text{ GeV/fm}^3$ for $\sqrt{s_{NN}} = 5.02 \text{ TeV}$ [7]. The other parameters, such as the initial momentum anisotropy, viscosity-to-entropy ratios, relaxation and thermalization times, are the same at all the mentioned collision energies at RHIC and LHC and at the same Laine-Schroeder equation of state [10] (the latter is only corrected to take into account a small chemical potential at the top RHIC energy as discussed below).

As for the initial momentum distribution for the pre-equilibrium dynamics, it is taken in

the following ‘‘Color-Glass-Condensate-like’’ form:

$$f_0(p) = g \exp \left(-\sqrt{\frac{(p \cdot U)^2 - (p \cdot V)^2}{\lambda_{\perp}^2} + \frac{(p \cdot V)^2}{\lambda_{\parallel}^2}} \right), \quad (2)$$

where $U^{\mu} = (\cosh \eta, 0, 0, \sinh \eta)$, $V^{\mu} = (\sinh \eta, 0, 0, \cosh \eta)$, η is space-time rapidity, and initial momentum anisotropy $\Lambda = \frac{\lambda_{\perp}}{\lambda_{\parallel}} = 100$ [1].

After the pre-thermal evolution in iHKM follows the viscous hydrodynamics stage, realized within the Israel-Stewart formalism. Here we describe the collisions at RHIC, so, in contrast to the LHC case, we need to account for a small, but still non-zero chemical potential (baryon and strange) in the equation of state (EoS) for the quark-gluon phase. In order to do this, we modify the EoS at zero chemical potential according to [11]:

$$\frac{p(T, \mu_B, \mu_S)}{T^4} = \frac{p(T, 0, 0)}{T^4} + \frac{1}{2} \frac{\chi_B}{T^2} \left(\frac{\mu_B}{T} \right)^2 + \frac{1}{2} \frac{\chi_S}{T^2} \left(\frac{\mu_S}{T} \right)^2, \quad (3)$$

where $p(T, 0, 0)$ is the Laine-Schroeder [10] equation of state at zero chemical potential and

$$\frac{\chi_i}{T^2} = \frac{1}{VT^3} \frac{\partial^2 \ln Z}{\partial (\mu_i/T)^2}, \quad i = B, S. \quad (4)$$

Here the ‘‘mixed’’ terms with χ_{BS} , as well as the terms proportional to electric chemical potential μ_E are neglected due to their smallness. In this paper we take $\mu_B = 21$ MeV at the hadronization/particlization hypersurface $T = 165$ MeV for the best description of the ratio of proton yield to that of antiproton for the centrality $c = 0 - 5\%$. And the value of $\mu_S = 5$ MeV is obtained using the variation method as satisfying the condition of zero strangeness on the hadronization (particlization) hypersurface:

$$S|_{\sigma_p} = 0, \quad S = \sum_i (N(i) - \bar{N}(i)) \mu_{S,i}, \quad (5)$$

where the sum is taken over all particle species, $N(i)$ is the number of particles of the i th sort, $\bar{N}(i)$ is the number of corresponding antiparticles on the hadronization hypersurface, and $\mu_{S,i}$ is the strange chemical potential of the particle species i . The evolution equations with chemical potential depending on T are considered in the same way as in Refs. [3, 4].

We assume that at the top RHIC energy the strange quarks do not have enough time to reach the chemical equilibrium in *non-central collisions*, so that the kaon spectra get down. The same concerns proton spectra, since about a half of produced protons come from the decays of strange resonances (such as Λ , Σ , Ξ). To take this into account we introduce an

centrality [%]	τ_p [fm/c]	γ_S
0-10	7.55	0.989
10-20	6.50	0.973
20-30	5.60	0.953
30-40	4.85	0.933
40-50	4.20	0.909
50-60	3.60	0.881
60-70	3.00	0.843
70-80	2.30	0.777

TABLE I. The values of γ_S for different centrality classes.

effective downscaling factor $\gamma_S(\tau_p)$, depending on the characteristic particlization time τ_p for each given centrality. This time is calculated in iHKM. Each hadron yield is multiplied by $\gamma_S^{S_i}$, where S_i is the strangeness of the hadron species i . We assume the dependence

$$\gamma_S(\tau_p) = A \exp(-b/\tau_p), \quad (6)$$

with $A = 1.1$ and $b = 0.8$ fm/c. This choice guarantees $\gamma_S = 1$ for the most central events and a good description of kaon and proton spectra, together with K/π ratio. Table I shows the gamma factors, obtained for different centralities based on the corresponding particlization times.

After the hydrodynamic stage in iHKM we have the particlization stage, when we switch from the description of the system's evolution in terms of continuous medium to the description in terms of particles. In the current analysis this switching is performed at the hadronization hypersurface $T = 165$ MeV. After that particles pass the stage of the hadronic cascade, realized in iHKM within the UrQMD model [12], which simulates resonance decays, as well as numerous elastic and inelastic hadron scatterings, taking place in expanding and initially dense hadronic gas.

III. RESULTS AND DISCUSSION

Having adjusted the model parameters and run enough simulations to collect good statistics, we can immediately calculate a great variety of observables, basing on the model output.

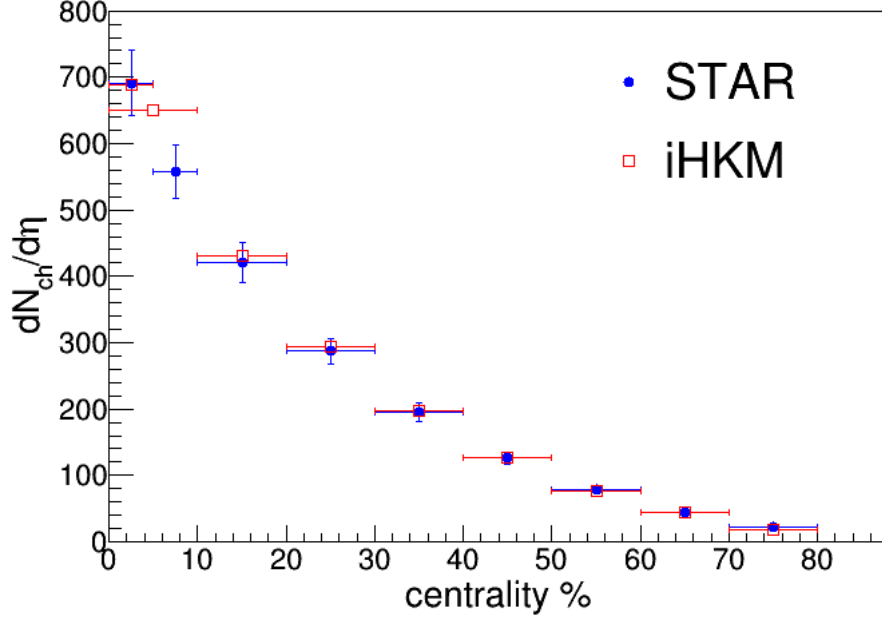


FIG. 1. The iHKM results on the mean charged particle density $\langle dN_{\text{ch}}/d\eta \rangle$ at $|\eta| < 0.5$ for different centrality classes, compared with the STAR data [13].

centrality [%]	$\langle dN_{\text{ch}}/d\eta \rangle$ in iHKM	$\langle dN_{\text{ch}}/d\eta \rangle$ from STAR
0-5	688	691 ± 49
10-20	431	421 ± 30
20-30	294	287 ± 20
30-40	197	195 ± 14
40-50	127	126 ± 9
50-60	77	78 ± 6
60-70	45	45 ± 3
70-80	19	22 ± 2

TABLE II. Mean charged particle density $\langle dN_{\text{ch}}/d\eta \rangle$ at $|\eta| < 0.5$ for different centrality classes.

In Fig. 1 and Table II one can see the iHKM results on the mean multiplicity of all charged particles $\langle dN_{\text{ch}}/d\eta \rangle$ in pseudorapidity range $|\eta| < 0.5$ for eight centrality classes — 0-5%, 10-20%, 20-30%, 30-40%, 40-50%, 50-60%, 60-70%, 70-80% — in comparison with the STAR experimental data [13]. The model results are in good agreement with the experiment.

In Fig. 2 we present our results on K^-/π^- and \bar{p}/π^- particle number ratios for different

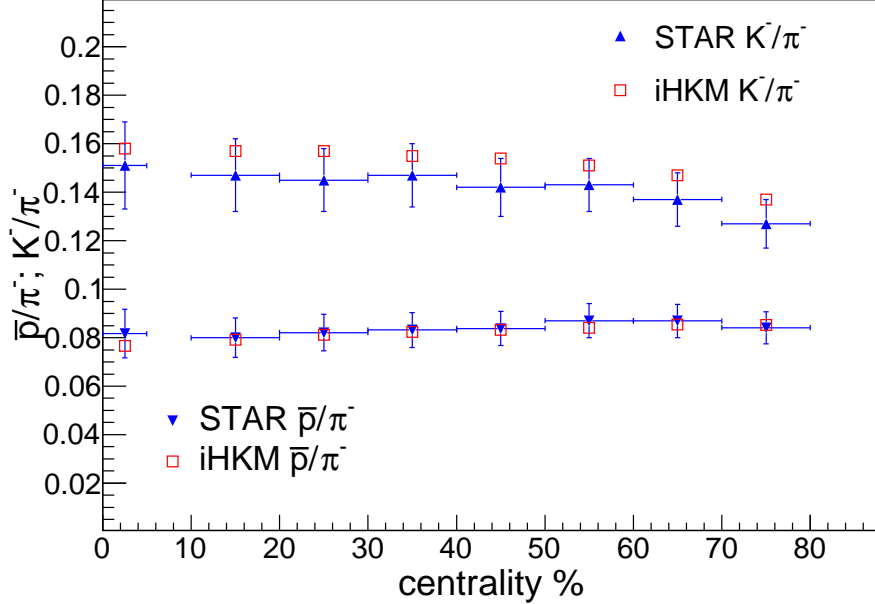


FIG. 2. The ratios of K^- (upper points) and \bar{p} (lower points) yields to that of π^- , obtained in iHKM in comparison with the STAR data [14]. Particles with $|y| < 0.1$ were selected for the analysis.

centrality classes in comparison with the experiment [14]. The hadrons with rapidity from the range $|y| < 0.1$ were selected to build all the ratios. As one can see from the figure, the iHKM describes well both ratios at all centralities within the errors, however K/π model points go through the upper edges of the experimental error bars.

Figures 3–6 demonstrate the iHKM description of transverse momentum spectra for negatively charged pions and kaons, as well as for protons and antiprotons at different centralities in the rapidity range $|y| < 0.1$. The simulation results are compared with the STAR experimental data [14]. One can say that the model reproduces the measured spectra quite well for all the mentioned particle species and all the centrality classes. A slight deviations of the iHKM lines from the experimental points can be noticed in K and \bar{p} spectra at low p_T for the very peripheral collisions with $c = 70 - 80\%$ only. Note however, that such a good agreement with data is achieved here using a “strangeness suppression” γ_S factor (6), which helps to lower the “raw” model kaon and (anti)proton spectra for non-central events.

In the next Fig. 7 for three centrality classes, $c = 10 - 20\%$, $c = 20 - 30\%$, and $c = 30 - 40\%$, we show the iHKM results on p_T -dependence of the elliptic flow, or v_2 coefficients, characterizing the anisotropy of the all-charged-particles transverse momentum spectra. The

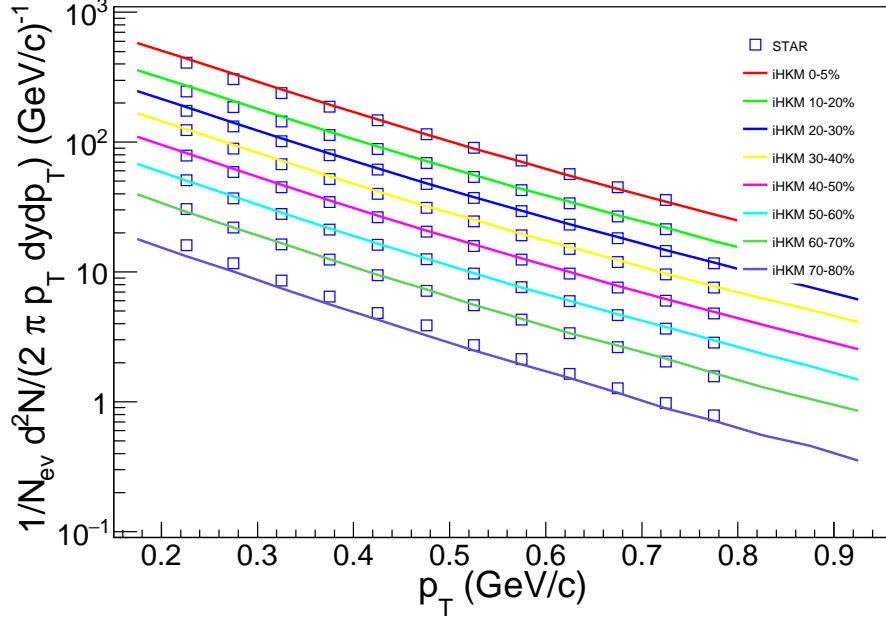


FIG. 3. The p_T spectra of π^- in comparison with the STAR data [14] at midrapidity, $|y| < 0.1$.

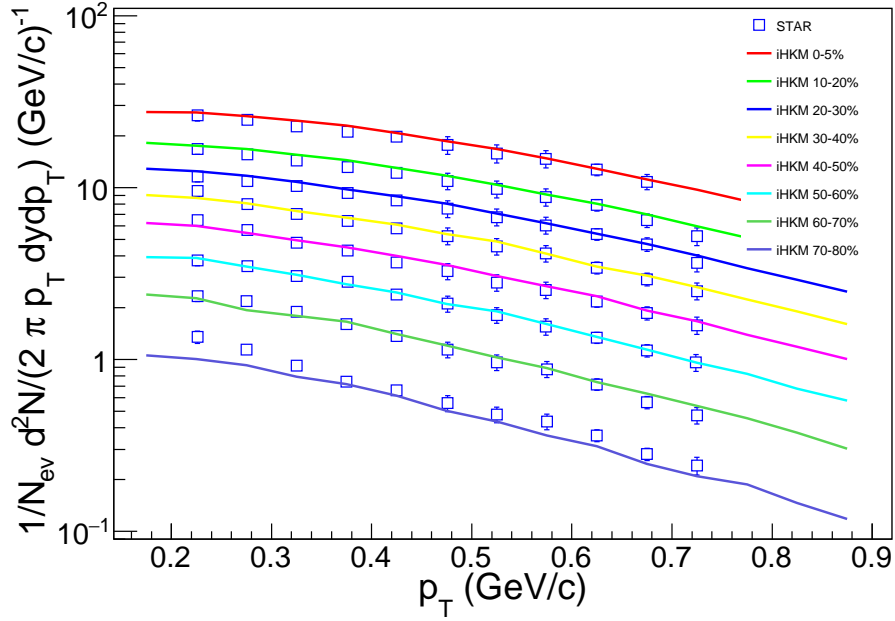


FIG. 4. The p_T spectra of K^- in comparison with the STAR data [14] at midrapidity, $|y| < 0.1$.

model lines go in agreement with data for not very high p_T .

In Figs. 8–11 one can find our results on the femtoscopy radii R_{out} , R_{side} , and R_{long} , extracted from the Gaussian fits to $\pi^-\pi^-$ and K^-K^- momentum correlation functions (CF).

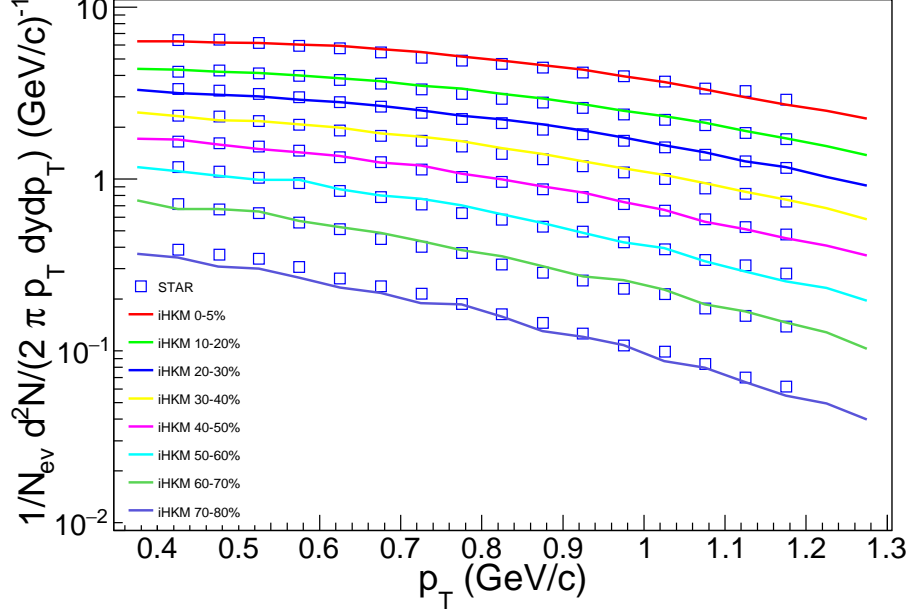


FIG. 5. The proton p_T spectra in comparison with the STAR data [14] at midrapidity, $|y| < 0.1$.

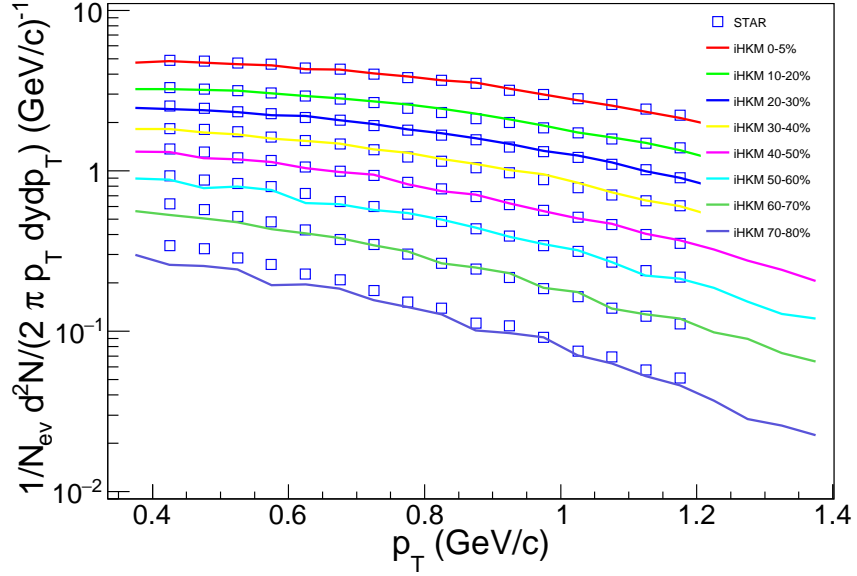


FIG. 6. The antiproton p_T spectra in comparison with the STAR data [14] at midrapidity, $|y| < 0.1$.

The dependencies of the interferometry radii on the mean pair transverse momentum k_T are presented for the four centrality classes: $c = 0 - 10\%$, $c = 10 - 20\%$, $c = 30 - 40\%$, and $c = 60 - 70\%$. All the correlation functions are built considering the specially selected

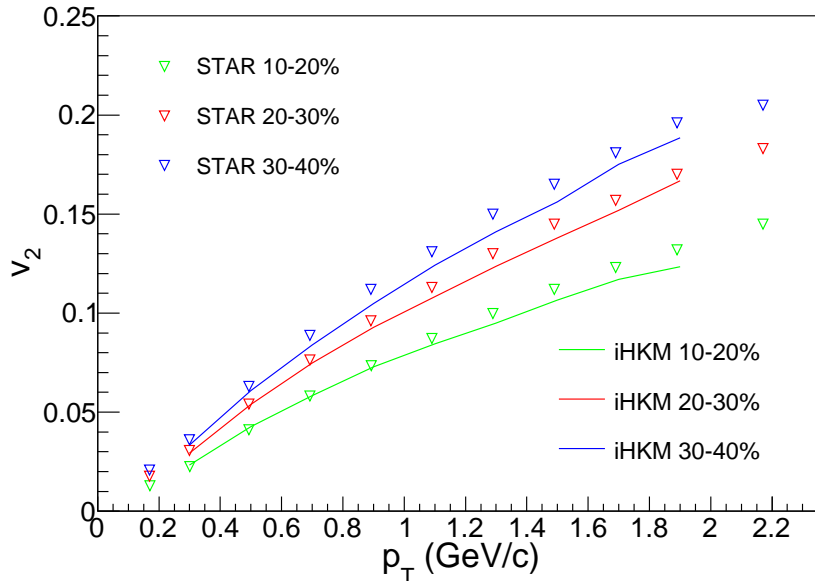


FIG. 7. The v_2 coefficients vs. p_T for all charged particles, calculated in iHKM (lines), together with the STAR data [15] (triangles). The results for the three centralities are shown: $c = 10 - 20\%$, $c = 20 - 30\%$, and $c = 30 - 40\%$.

particles with $0.15 < p_T < 1.55$ GeV/ c and $|\eta| < 1$.

In the first two figures, the iHKM results for the two centralities, $c = 0 - 10\%$ and $c = 10 - 20\%$, are compared with the experimental data on pion and kaon femtoscopy scales from the PHENIX [5] and the STAR [2, 16] collaborations. The STAR data for KK pairs [2] are preliminary. From the plots it is clear, that iHKM gives a good description of $R_{\text{long}}(k_T)$ dependency both in $\pi\pi$ and in KK case. As for R_{out} and R_{side} radii, the situation seems to be not so nice. The model lines for KK look well, but for $\pi\pi$ pairs we see that R_{out} values are overestimated, especially for $c = 0 - 10\%$, while R_{side} values are, conversely, underestimated, most noticeably at high k_T . As a result, we obtain a rather overestimated $R_{\text{out}}/R_{\text{side}}$ ratio in pion case.

Also, looking at the figures, one could say that at least R_{side} and R_{long} iHKM curves demonstrate something like scaling between pions and kaons at high k_T . For the LHC energies such k_T -scaling at $k_T > 0.4$ GeV/ c for all radii was previously noticed in iHKM simulations [7, 17] and then for $\sqrt{s_{NN}} = 2.76$ TeV Pb+Pb collisions confirmed in the ALICE experimental paper [18].

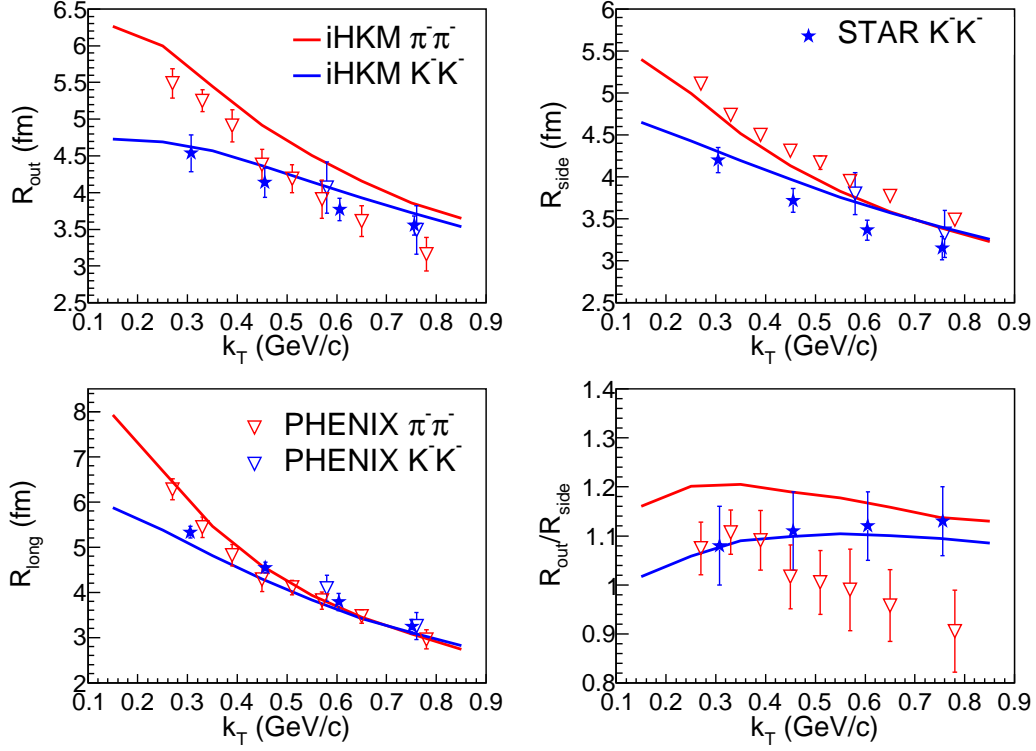


FIG. 8. The iHKM results on $\pi^-\pi^-$ and K^-K^- femtoscopy scales vs. pair k_T (lines) in comparison with the experimental data from PHENIX [5] (triangles) and STAR [2, 16] (stars) for the events from the centrality class $c = 0 - 10\%$. Red color is related to pions, blue color is related to kaons.

In addition, in this paper we apply for the top RHIC energy the method, proposed for the LHC case in [19] and successfully applied in [18], that allows one to extract pion and kaon maximal emission times, τ_π and τ_K , having their p_T spectra and $R_{\text{long}}(m_T)$ dependencies.

At first we perform a combined fit to pion and kaon transverse momentum spectra, using the analytical formula from [19]:

$$p_0 \frac{d^3 N}{d^3 p} \propto \exp[-(m_T/T + \alpha)(1 - \bar{v}_T^2)^{1/2}]. \quad (7)$$

Here T is the effective temperature, α is a parameter, characterizing the intensity of collective flow (the infinite α means absent flow, while small α values mean strong flow), and \bar{v}_T is the flow transverse velocity at the saddle point, $\bar{v}_T = k_T/(m_T + \alpha T)$ (see [19] for details). The spectra fitting is done in p_T range $0.45 < p_T < 1.0$ GeV/ c . As a result, we obtain $T = 141$ MeV as a common temperature value for both pions and kaons, and two α values, $\alpha_\pi = 7.86 \pm 2.11$ and $\alpha_K = 5.54 \pm 2.61$, for each hadron species respectively.

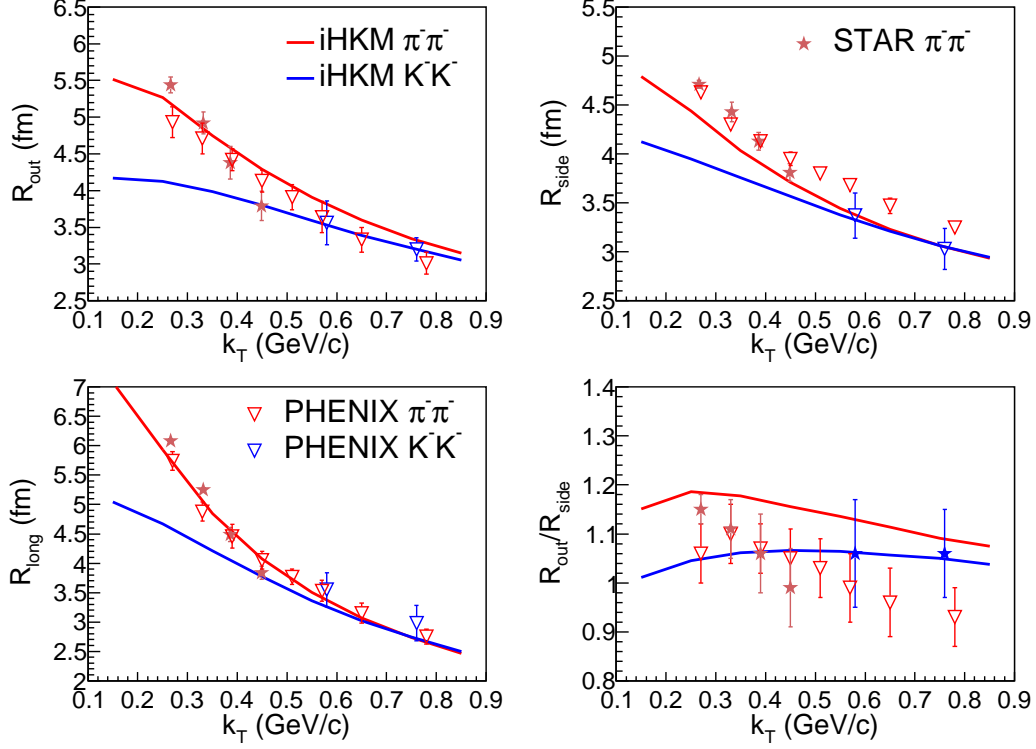


FIG. 9. The same as in Fig. 8 for the centrality class $c = 10 - 20\%$.

After that we use another formula from [19] to fit kaon and pion $R_{\text{long}}(m_T)$ dependencies:

$$R_{\text{long}}^2(m_T) = \tau^2 \lambda^2 \left(1 + \frac{3}{2} \lambda^2 \right), \quad (8)$$

where λ is connected with the system's homogeneity length in longitudinal direction λ_l , namely $\lambda^2 = (\lambda_l/\tau)^2 = T/m_T \cdot (1 - \bar{v}_T^2)^{1/2}$, and τ is the corresponding maximal emission time. Our values of R_{long} radii were obtained from Gaussian fits to the corresponding correlation functions in the particle momentum difference q interval $|q| < 0.3$ GeV/ c .

Then, having constrained the T and α parameters according to the results of combined p_T -spectra fitting, we extract the desired maximal emission time $\tau_\pi = 7.12 \pm 0.01$ fm/ c for pions from the fit to pion $R_{\text{long}}(m_T)$ dependency using the formula (8). In order to obtain the τ value for kaons, similarly to the LHC case, described in [19], we have to set α parameter free at fitting kaon R_{long} points. Eventually, we obtain maximal emission time $\tau_K = 9.71 \pm 0.02$ fm/ c , and the kaon α value $\alpha_K = 0.12 \pm 0.02$. One can see both iHKM $R_{\text{long}}(m_T)$ dependencies together with fits to them in Figs. 12, 13.

Finally, in Fig. 14 we present the iHKM pion and kaon averaged emission functions

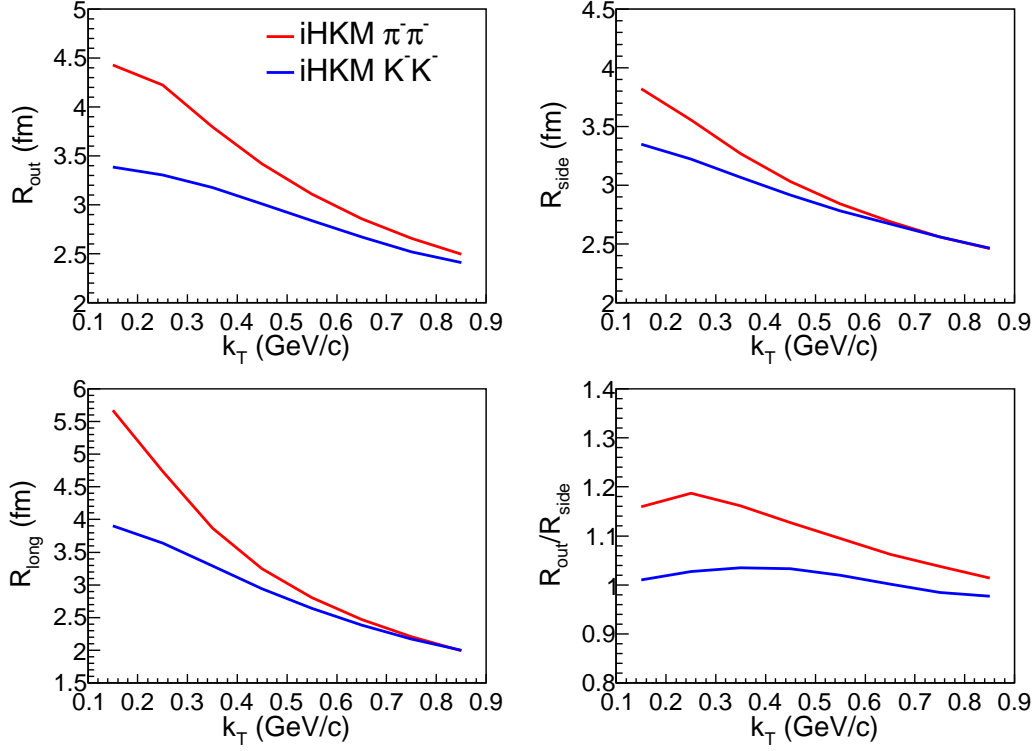


FIG. 10. The same as in Fig. 8 for the centrality class $c = 30 - 40\%$.

$g(\tau, r_T, p_T)$, which reveal the space-time picture of radiation of these particles. The maximal emission times can be approximately found from these plots, if one attributes some τ values to the regions, where each $g(\tau, r_T, p_T)$ has maximum. As it is readily seen, maximal emission time values obtained in this way are close to those accurately extracted from fits. More detailed analysis, provided in Ref. [20], shows that the reason for a larger time of maximal emission, obtained for kaons, as compared with pions, is in intensive decays and recombinations of K^* mesons (having life-time near $4 \text{ fm}/c$), which take place at the afterburner stage of the collision. This effect was also found in the ALICE experimental analysis [18].

IV. CONCLUSIONS

The integrated hydrokinetic model showed itself not less successful in describing the variety of bulk observables in Au+Au collisions at the top RHIC energy, than in Pb+Pb ones at the available LHC energies. After adjusting the main model parameters, namely

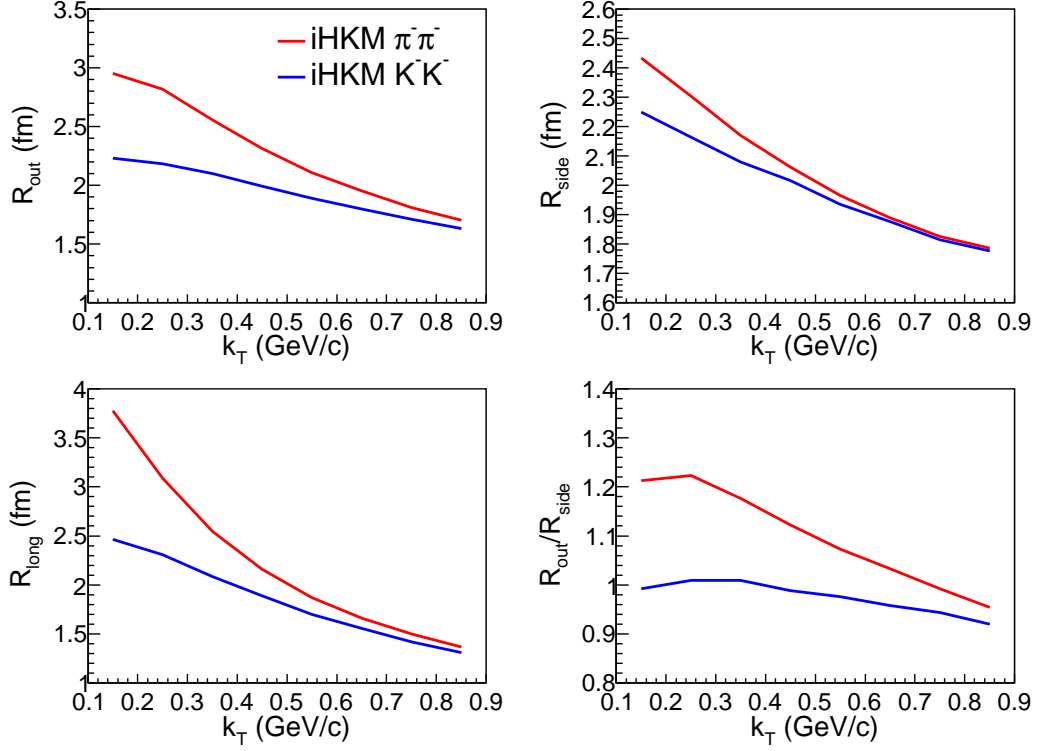


FIG. 11. The same as in Fig. 8 for the centrality class $c = 60 - 70\%$.

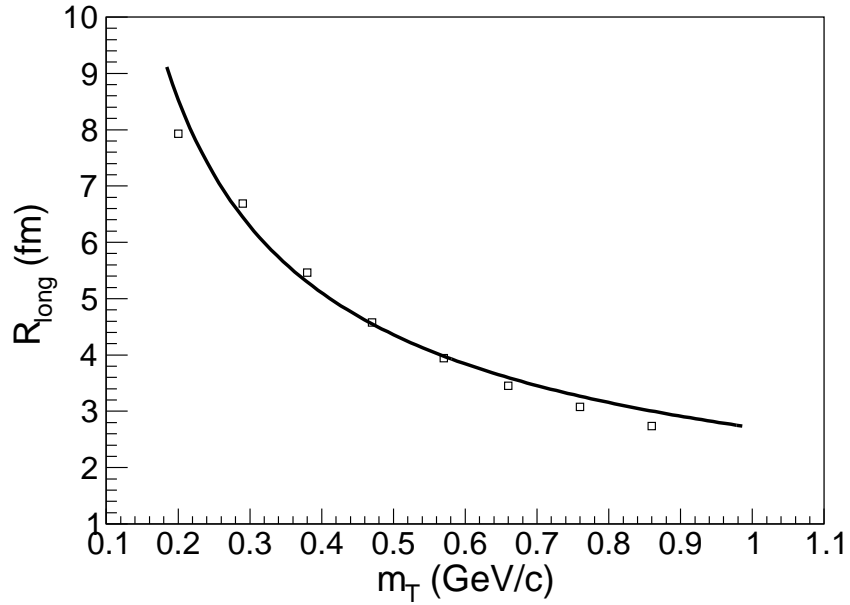


FIG. 12. The R_{long} dependency on pair m_T for the negatively charged pion pairs together with the fit to it according to formula (8).

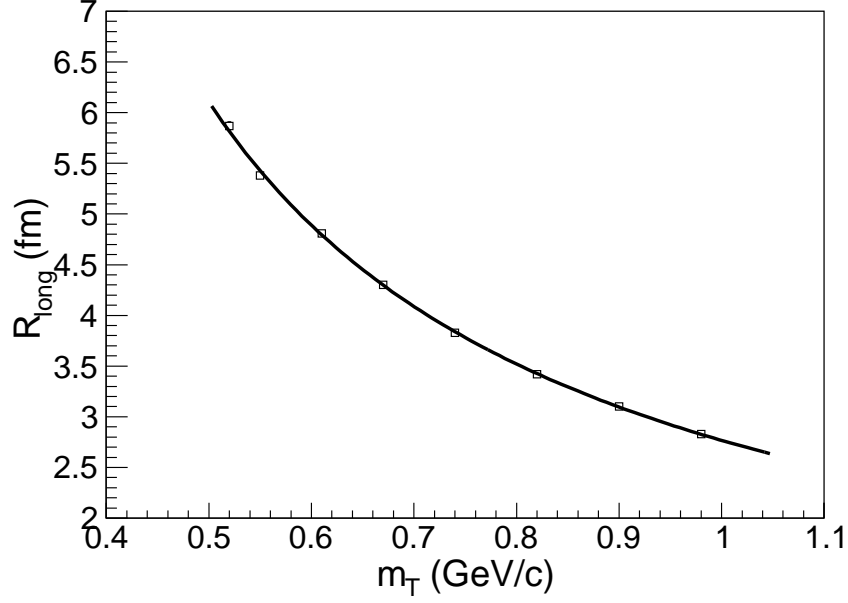


FIG. 13. The same as in Fig. 12 for negatively charged kaon pairs.

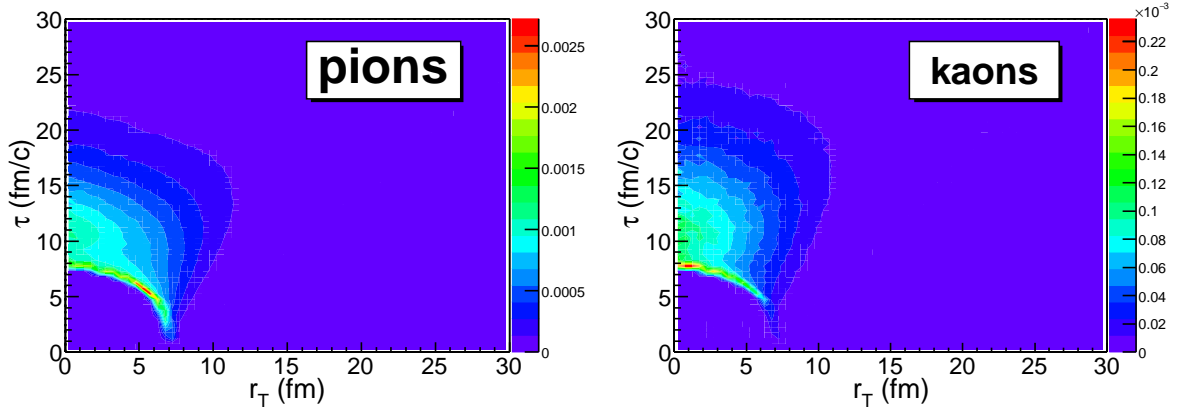


FIG. 14. The pion and kaon emission functions $g(\tau, r_T, p_T)$ [fm^{-3}], averaged over complementary variables, obtained from iHKM for the centrality class $c = 0 - 10\%$. Particles with $0.2 < p_T < 0.3$ GeV/ c and $|\eta| < 1$ were chosen for the analysis.

the maximal initial energy density $\epsilon_0(\tau_0)$ and the binary collision contribution to the initial transverse energy-density profile α , the iHKM allowed to describe simultaneously the experimental particle yields and their ratios, p_T spectra for pions, kaons and (anti)protons, and v_2 coefficients for all charged particles.

As for the femtoscopy scales, they are described in the model well for kaon pairs, and in the pion case we observe some overestimation of R_{out} and underestimation of R_{side} radius, more pronounced at high pair k_T .

The longitudinal radii R_{long} perfectly describe the experimental data at different centralities. So, they are used to extract the times of the maximal emission for pions and kaons according to the procedure, proposed for the LHC case in the paper [19]. We found that both corresponding times are about 2 fm/ c less than at the LHC energy $\sqrt{s_{NN}} = 2.76$ TeV. Similarly as at the LHC, the maximal emission time for kaons is larger than for pions. And again, we explain the latter fact by the intensive decays and recombinations of K^* resonances at the final stage of the collision.

ACKNOWLEDGMENTS

The research was carried out within the scope of the EUREA: European Research Network “Heavy ions at ultrarelativistic energies” and corresponding Agreement with the National Academy of Sciences (NAS) of Ukraine. The work is partially supported by the NAS of Ukraine Targeted research program “Fundamental research on high-energy physics and nuclear physics (international cooperation)”. The publication contains the results of studies conducted by President’s of Ukraine grant for competitive projects (project number F75/219-2018) of the State Fund for Fundamental Research.

-
- [1] V.Yu. Naboka, Iu.A. Karpenko, Yu.M. Sinyukov, Phys. Rev. C **93**, 024902 (2016).
 - [2] G. Nigmatkulov, arXiv:1712.09964v1.
 - [3] Iu.A. Karpenko, Yu.M. Sinyukov, Phys. Rev. C **81**, 054903 (2010)
 - [4] Iu.A. Karpenko, Yu.M. Sinyukov, K. Werner. Phys. Rev. C **87**, 024914 (2013).
 - [5] A. Adare *et al.* (PHENIX Collaboration), Phys. Rev. C **92**, 034914 (2015).
 - [6] Yu.M. Sinyukov, V.M. Shapoval, Phys. Rev. C **97**, 064901 (2018).
 - [7] V.M. Shapoval, Yu.M. Sinyukov, arXiv:1809.07400 [hep-ph].
 - [8] V.Yu. Naboka, S.V. Akkelin, Iu.A. Karpenko, Yu.M. Sinyukov, Phys. Rev. C **91**, 014906 (2015).

- [9] W. Broniowski, M. Rybczynski, P. Bozek, *Comput. Phys. Commun.* **180**, 69 (2009).
- [10] M. Laine and Y. Schroeder, *Phys. Rev. D* **73**, 085009 (2006).
- [11] F. Karsch, arXiv:0711.0656.
- [12] S.A. Bass et al., *Prog. Part. Nucl. Phys.* **41**, 255 (1998); M. Bleicher et al., *J. Phys. G* **25**, 1859 (1999).
- [13] B.I. Abelev *et al.* (STAR Collaboration), *Phys. Rev. C* **79**, 034909 (2009).
- [14] J. Adams et al. (STAR Collaboration), *Phys. Rev. Lett.* **92**, 112301 (2004).
- [15] J. Adams *et al.* (STAR Collaboration), *Phys. Rev. C* **72**, 014904 (2005).
- [16] J. Adams *et al.* (STAR Collaboration), *Phys. Rev. C* **71**, 044906 (2005).
- [17] V.M. Shapoval, P. Braun-Munzinger, Iu.A. Karpenko, Yu.M. Sinyukov, *Nucl. Phys. A* **929**, 1 (2014).
- [18] J. Adam *et al.* (ALICE Collaboration), *Phys. Rev. C* **96**, 064613 (2017).
- [19] Yu.M. Sinyukov, V.M. Shapoval, V.Yu. Naboka, *Nucl. Phys. A* **946**, 227 (2016).
- [20] V.M. Shapoval, P. Braun-Munzinger, Yu.M. Sinyukov, *Nucl. Phys. A* **968**, 391 (2017).